Supporting Information

Nagy *et al*. 10.1073/pnas.0802592105

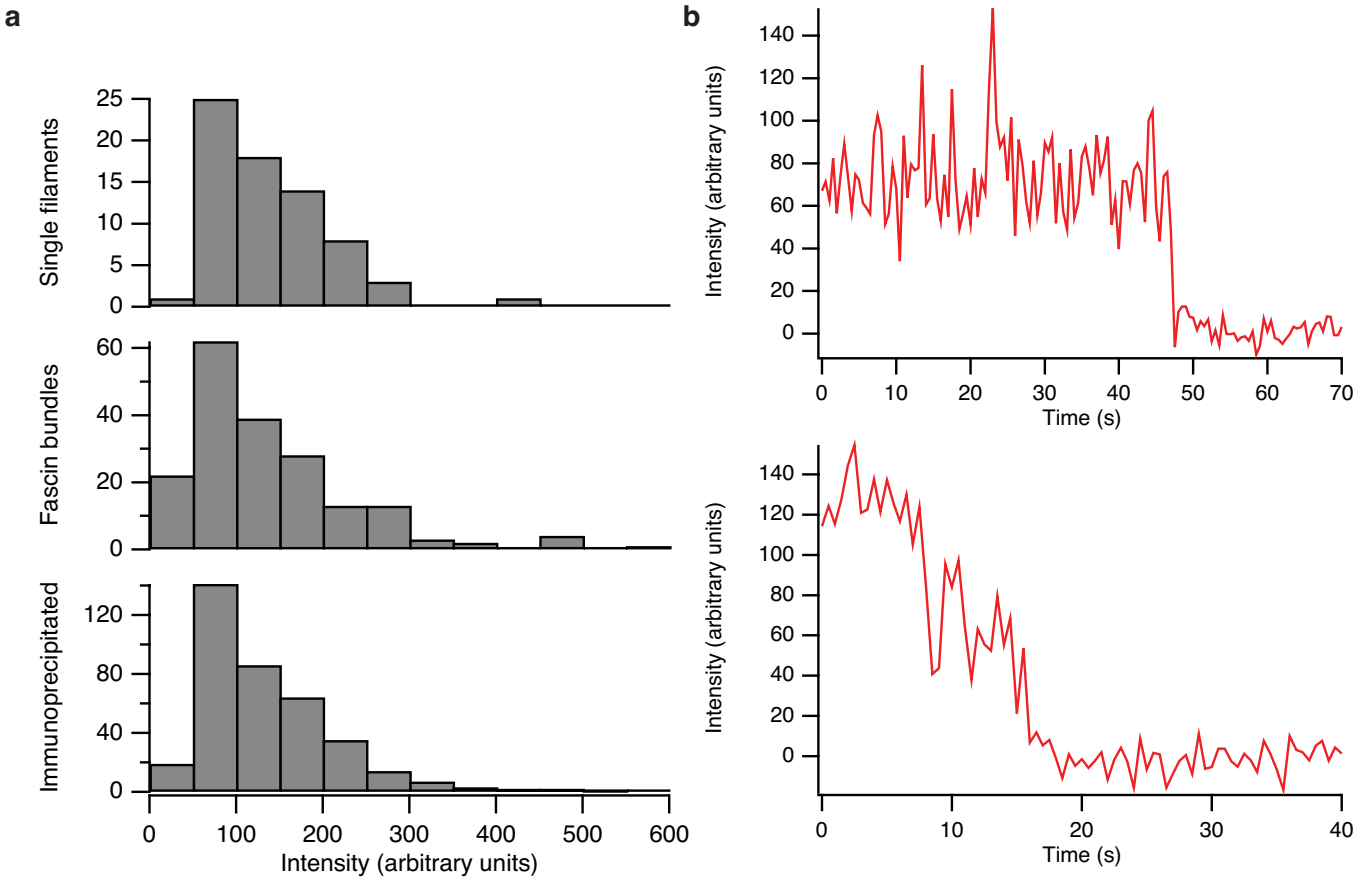

Fig. S1. Single-molecule fluorescence imaging. (*a*) Initial intensity distributions of the forced dimer. Cy5 spot intensities were measured for moving motors on actin or actin bundles, and for immunoprecipitated motor (via an anti-GFP antibody). Photobleaching events for immobilized myosin X were processed by tabulating the intensity of a 7×7 pixel area for each spot, over 200 frames. Initial intensity distributions of the labeled myosin X were determined by averaging the first 5 frames of the photobleaching experiment and subtracting the average of the last 5 frames, after the spot has completely bleached. For the intensity distribution of moving spots, the first 5 frames of moving spots were averaged and subtracted from the background after the spot had bleached. We did not observe any significant difference between the three distributions, suggesting that moving spots are representative of the bulk sample (tested by the two-tailed Wilcoxon rank-sum test at the $\alpha = 0.1$ level, *P* values: immunoprecipitated vs. bundles, $P = 0.14$; immunoprecipitated vs. singles, $P = 0.37$; bundles vs. singles, $P = 0.17$). We observe between one and five stepwise photobleaching events for Cy5, less than the six calmodulins per forced dimer. (*b*) Example photobleaching traces of GFP on the forced dimer. Traces are shown for surface-adsorbed forced dimer. GFP bleached in at most two steps, as expected for the forced dimer.

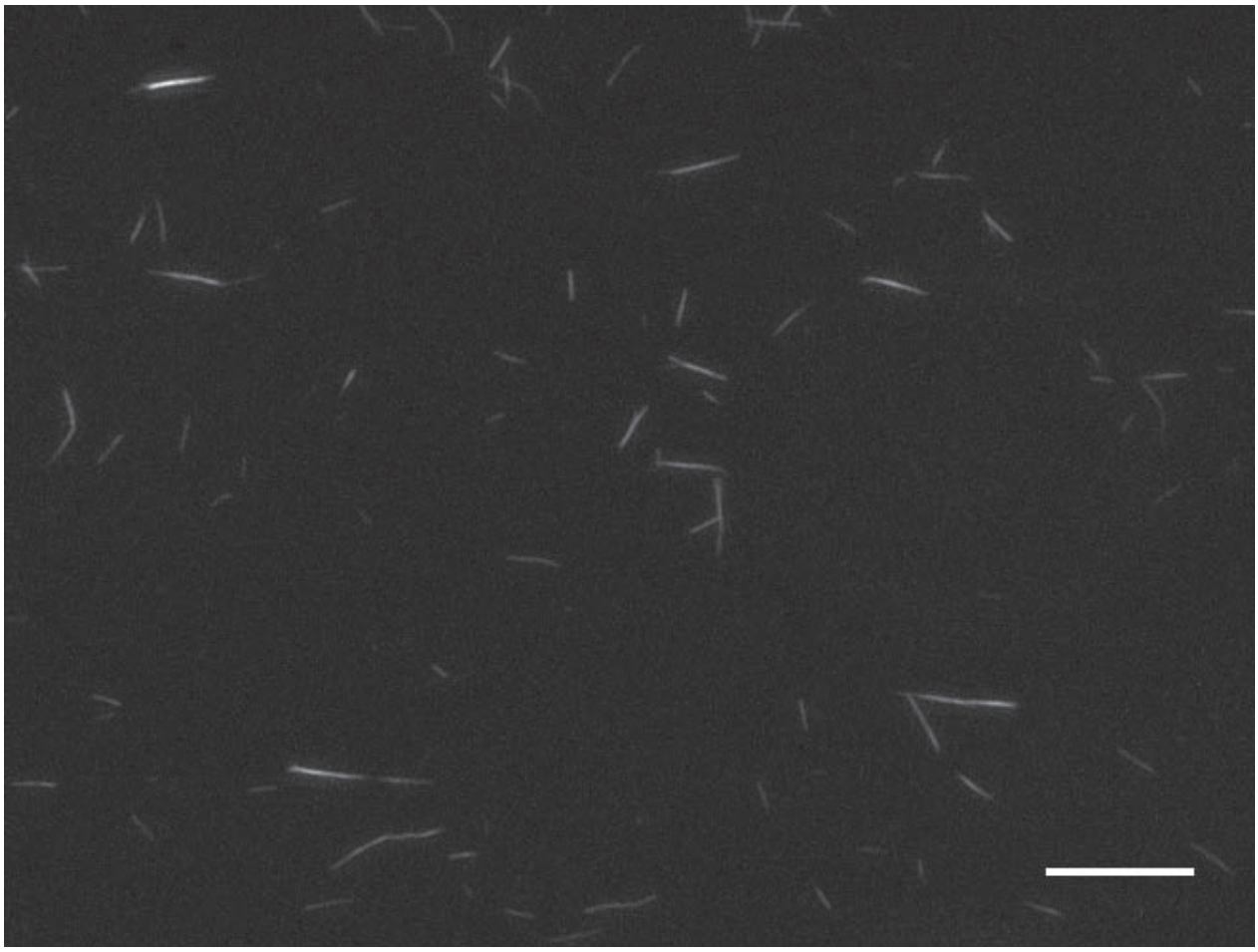

Fig. S2. A low magnification, epifluorescence image of the fascin-actin bundles, at the density used in the TIRF experiments of Fig. 2. (Scale bar, 25 μm.)

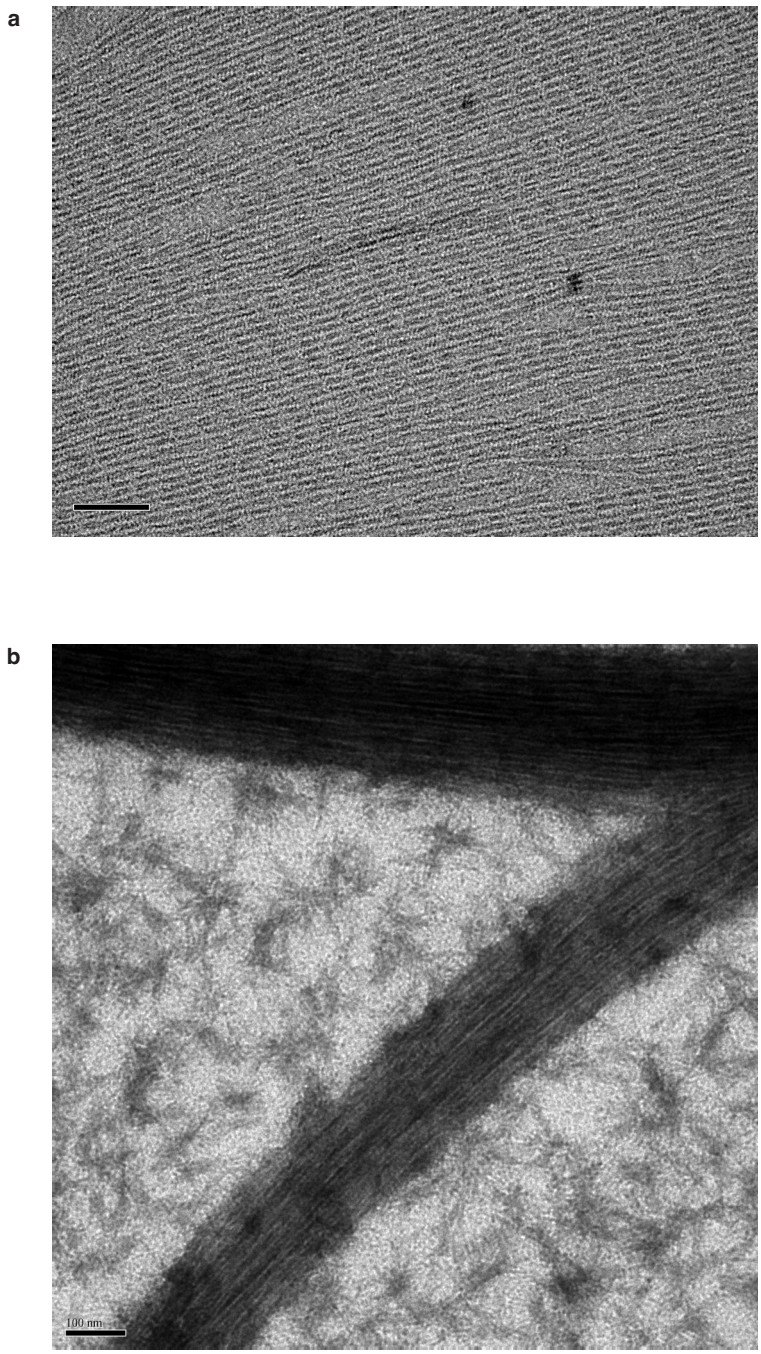

Fig. S3. Electron micrographs of actin bundles. (*a*) Electron microscopy of actin filaments in a fascin bundle. To facilitate this analysis, we used two-dimensional paracrystalline arrays of actin filaments with the incorporation of a bundling protein, exactly as decribed by Taylor and Taylor [Taylor KA, Taylor DW (1994) Formation of two-dimensional complexes of F-actin and crosslinking proteins on lipid monolayers: Demonstration of unipolar alpha-actinin-F-actin crosslinking. *Biophys J* 67:1976–1983]. The samples were stained with uranyl acetate, and micrographs obtained with an FEI Tecnai F30 scanning transmission electron microscope. The interfilament spacing of ≈11.5 nm (center-to-center) was measured by drawing a line normal to the long axis of the filaments in a region of coherent parallel arrangement with clear fascin incorporation and calculating the total calibrated length per filament. Thus, the gap between filaments is ≈3.5 nm. The image here is a typical example of such an actin sheet with incorporated fascin. (Scale bar, 100 nm.) (*b*) Electron microscopy of methylcellulose bundles. Bundles were prepared in solution from Limulus sperm acrosomal processes and methylcellulose according to the methods given in the main text. The bundles were transferred to carbon-coated EM grids and stained with uranyl acetate. The individual actin filaments are in close proximity, with an average spacing of ≈10 nm (center-to-center), for a ≈2 nm gap between filaments. We expect that this spacing is highly dynamic under the motility assay conditions. The amorphous material between the bundles is likely methylcelluose, and does not appear in control grids. (Scale bar, 100 nm.)

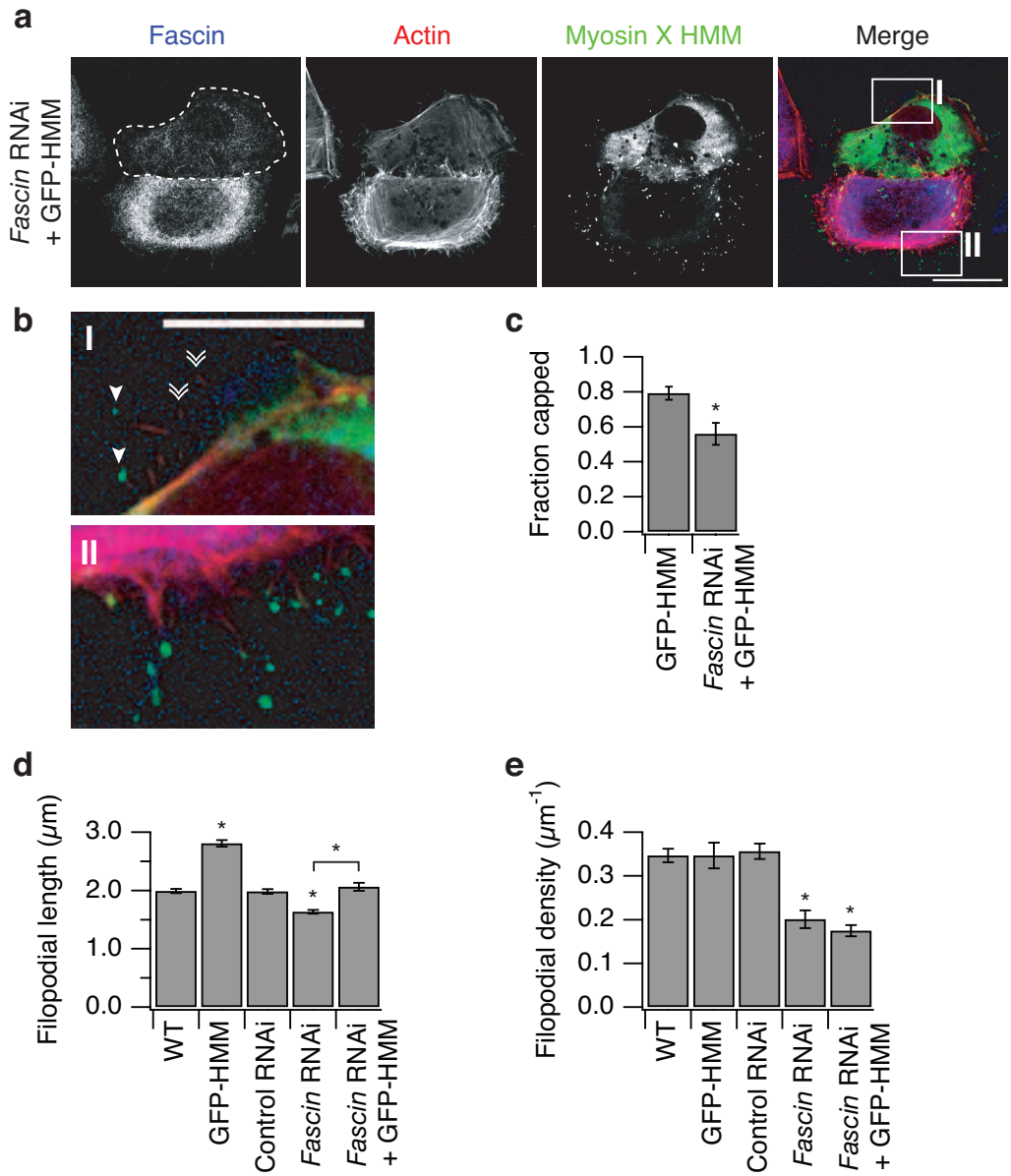

Fig. S4. Fascin is required for *in vivo* localization of exogenous GFP-myosin X. (*a*) Z-projection of three confocal sections of HeLa cells expressing myosin X GFP-HMM, immunostained for fascin, and phalloidin stained for actin. We identified cells transfected with the fascin RNAi hairpin by their reduced fascin levels (dotted outline) compared to neighboring untransfected cells. (Scale bar, 20 μm.) (*b*) Detail of confocal projection in *a*. Region I shows a segment of the cell perimeter of the fascin-depleted cell. Single arrowheads mark filopodia in the depleted cell that contain GFP-HMM at the tip, and double arrowheads mark filopodia that lack GFP-HMM at the tip. Region II shows a segment of the neighboring cell with wild-type fascin levels. (Scale bar, 10 μm.) (*c*) Fascin-depletion reduces filopodial capping by myosin X. The fraction of filopodia with GFP-HMM at the tip is shown. Capping was measured on a cell-by-cell basis and averaged across cells (n = 21 cells each, ± SEM, P = 0.005). (*d*) Fascin-depletion inhibits filopodial growth. Fascin-depleted cells show a decrease in filopodial length (n = 400–526 filopodia each, ±SEM, $P < 1 \times 10^{-10}$), similar to Vignjevic (10). Transfection with GFP-HMM increases filopodial length of wild-type and, to a lesser extent, fascin-depleted cells (n = 350–1,000 filopodia each, ±SEM). For both wild-type and fascin-depleted cells, capped filopodia are longer than uncapped filopodia (n = 151–357 each, $P < 2 \times 10^{-10}$ for wild type, $P < 0.00015$ for fascin-depleted). (*e*) Fascin RNAi reduces the filopodial density. The mean number of filopodia per μm of nonoverlapping cell perimeter is shown for cells transfected with the indicated constructs. The fascin RNAi results in fewer filopodia than either wild-type or control RNAi, similar to Vignjevic (10). Exogenous GFP-HMM does not increase density for either the wild-type or the fascin RNAi cells. Densities were measured on a cell-by-cell basis and averaged across cells (n = 21 cells each, ± SEM). In *d* and *e*, significant differences compared to wild-type (unless indicated) are marked with an asterisk (see Table S1 for P values). *Fascin* RNAi transfection and plating were performed as in Fig. 3, with the addition of transfection with GFP-HMM (5) 22 h before plating. Cells were fixed with 4% paraformaldehyde for 20 min; permeabilized in 0.5% Tween 20; blocked with 5% FBS; incubated overnight at 4°C with mouse anti-fascin (DakoCytomation), 1 h at room temperature with Cy5 goat anti-mouse (ChemiCon), and 30–60 min with 25 nM TRITC-phalloidin (Sigma) with PBS washes between incubations. Images were collected on Zeiss LSM-510 confocal microscope with a z-step of 0.4 μm. We counted surface attached filopodia (visible in the actin channel) extending at least 0.5 μm beyond the cell perimeter in ImageJ. Error bars are the standard errors derived from 1000 bootstrap samples drawn from the individual datasets.

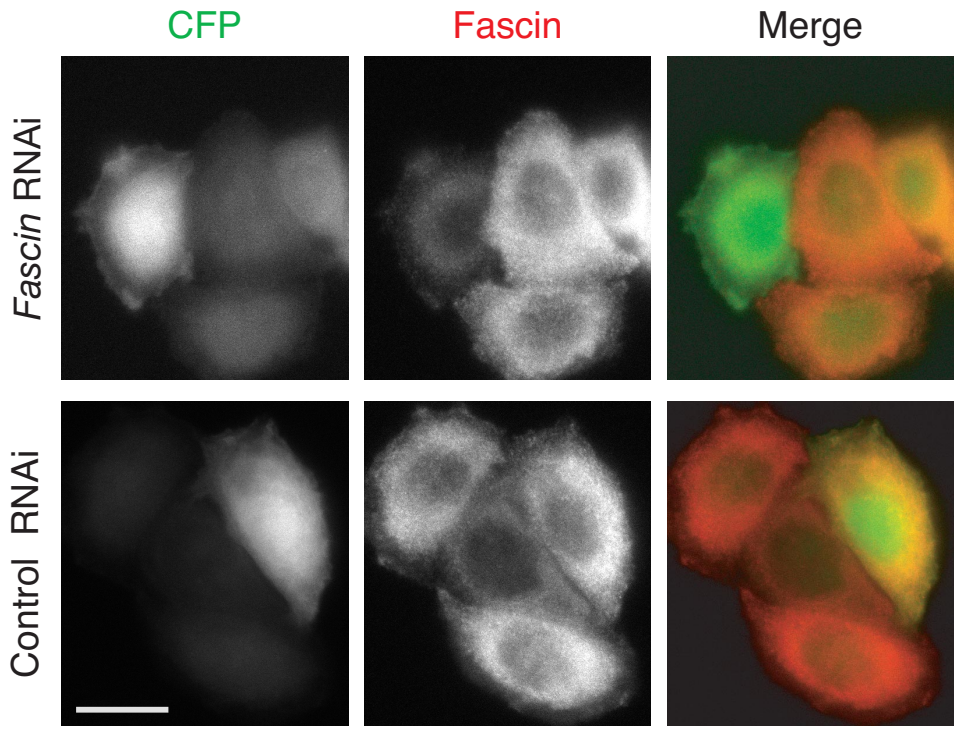

Fig. S5. Fascin depletion in HeLa cells. (*Upper*) Five days after transfection with a *fascin* shRNA plasmid containing a CFP marker, fascin levels in transfected cells are reduced to 23 ± 7% (SD, $n = 10$ cells) of the wild-type level. (*Lower*) Five days after transfection with a control shRNA plasmid (targets mouse fascin but not human), also containing a CFP marker, fascin levels are similar in transfected and untransfected cells. Cells were fixed and stained for fascin as in Fig. S4, and were imaged in epifluorescence on a Zeiss Axio Imager.M1 by a Photometrics Cascade 1k CCD. Scale bar, 20 μm.

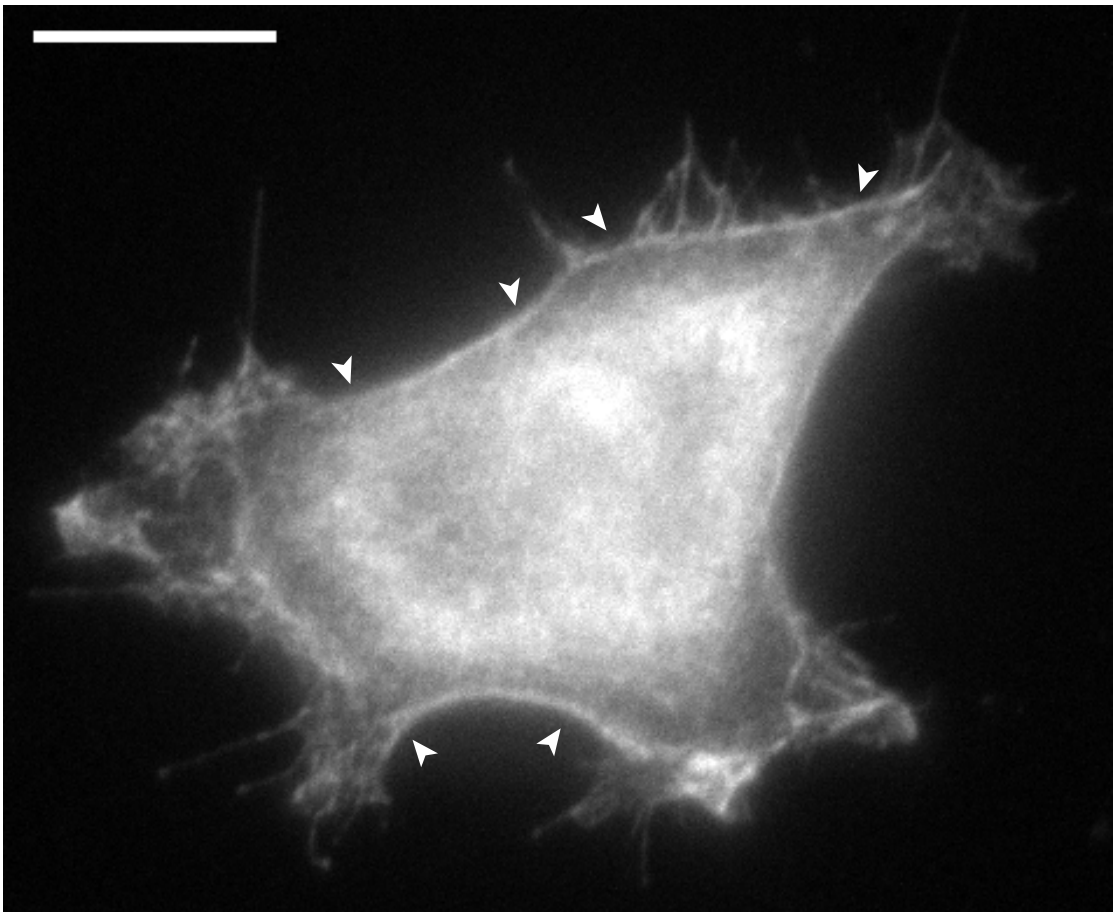

Fig. S6. Epifluorescence image of fascin immunostained wild-type HeLa cell illustrates that some fascin-rich structures run parallel to the plasma membrane (indicated by arrowheads). These structures could support the lateral motility of myosin X reported previously (1, 2). (Scale bar, 10 μm.)

1. Sousa AD, Berg JS, Robertson BW, Meeker RB, Cheney RE (2006) Myo10 in brain: developmental regulation, identification of a headless isoform and dynamics in neurons. *J Cell Sci* 119:184–194.
2. Tokuo H, Mabuchi K, Ikebe M (2007) The motor activity of myosin-X promotes actin fiber convergence at the cell periphery to initiate filopodia formation. *J Cell Biol* 179:229–238.

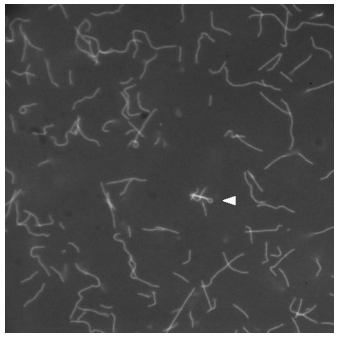

Movie S1. This movie shows gliding filament *in vitro* motility of myosin X. Numerous plectonemes are formed throughout the field (indicated by arrowheads) as myosin X twists the actin filaments. The time lapse covers a period of ≈100 s, and shows a 30 × 30 μm area. (QuickTime; 5 MB).

Movie S1 (MOV)

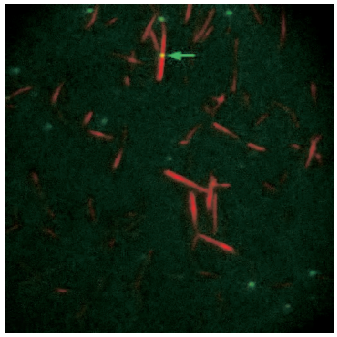

Movie S2. This movie shows single-molecule motility of myosin X (green) on fascin-actin bundles (red). Numerous long runs are observed. The time lapse covers a period of ≈100 s, and shows a 30 × 30 μm area. (QuickTime; 4 MB).

Movie S2 (MOV)

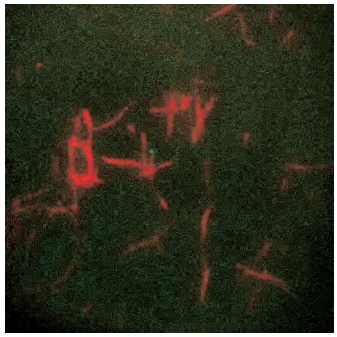

Movie S3. This movie shows single-molecule motility of myosin X (green) on single actin filaments (red). The majority of events are simple binding and release. The total actin concentration is one-tenth that of Movie S2. The time lapse covers a period of ≈100 s, and shows a 30 × 30 μm area. (QuickTime; 4 MB).

Movie S3 (MOV)

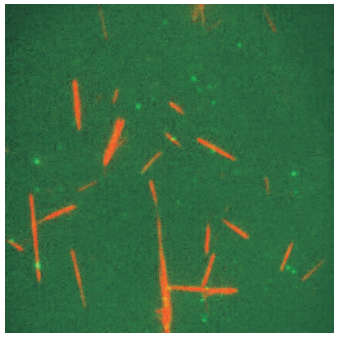

Movie S4. This movie shows single-molecule motility of nmIIb myosin (green) on fascin-actin bundles (red). All events are simple binding and release. The time lapse covers a period of ≈200 s, and shows a 30 × 30 μm area. (QuickTime; 4 MB).

Movie S4 (MOV)

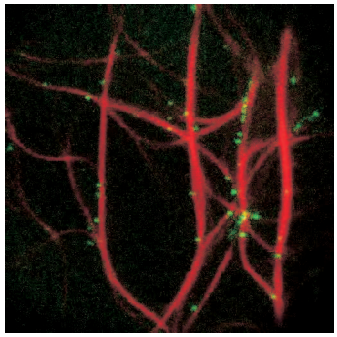

Movie S5. This movie shows single-molecule motility of myosin X (green) on methycellulose-bundled actin (red). Actin filaments in this system assemble into large cables that branch and merge. Some of these bundles are unidirectional and support high-speed motility with long runs (e.g., the central, vertical bundle). Others are likely mixed polarity, as some back-and-forth motions are observed. (QuickTime; 4 MB).

Movie S5 (MOV)

Table S1. *P* values for filopodial measurements

	Filopodial density (Fig. S4)	Filopodial lengths (Fig.S3)
HMM vs. WT	0.82 (n =21, 21)	**<0.001** (n = 721, 1029)
Control RNAi vs. WT	0.78 (n =21, 21)	0.35 (n = 831, 1029)
Fascin RNAi vs. WT	**<0.001** (n =21,21)	**<0.001** (n = 455, 1029)
Fascin RNAi + HMM vs. WT	**<0.001** (n =21,21)	0.38 (n = 347, 1029)
Fascin RNAi vs. Fascin RNAi + HMM	0.56 (n =21, 21)	**<0.001** (n = 455, 347)

P values from the two-tailed Wilcoxon rank-sum test. Significant differences are indicated in bold, at the $\alpha = 0.002$ level (applying the Bonferroni correction for five tests). Dataset sizes are for the first and second listed datasets, respectively.